ELSEVIER

Biochimica et Biophysica Acta 1234 (1995) 52–62

BBA Biochimica et Biophysica Acta

Observation of extremely heterogeneous electroporative molecular uptake by *Saccharomyces cerevisiae* which changes with electric field pulse amplitude

Elizabeth A. Gift, James C. Weaver *

Harvard-M.I.T. Division of Health Sciences and Technology, Massachusetts Institute of Technology, Cambridge, MA 02139, USA

Received 10 August 1994; accepted 26 October 1994

Abstract

Molecular uptake of a charged fluorescent molecule (calcein; 623 Da, $z = -4$) was quantitatively determined at the single cell level using flow cytometry. Dilutely suspended cells were exposed to one exponential pulse ($\tau_p \approx 300$ μs) for different field strength values. For an asymmetric cell such as the yeast *Saccharomyces cerevisiae* a significant variation in the number of molecules taken up by individual cells was expected for physical reasons. By carrying out several thousand individual cell measurements for each pulse condition, we found that the number of molecules per cell varies significantly within the cell population, and that this population distribution changes markedly as the field strength is varied. Surprisingly, in spite of significant changes in this distribution with field strength, the average uptake per cell reaches a non-equilibrium plateau for which the uptake per cell is much smaller than the product of the mean cell volume and the supplied extracellular concentration. These observations of different field-dependent cell population distributions of uptake support the hypotheses that (1) electroporation is a transmembrane voltage-responsive phenomenon, so that cells of different sizes, shapes and orientation, respond differently to even a spatially uniform applied field, (2) population average measurements of electroporation behavior can be incomplete and misleading, and (3) transport of small charged molecules is due to electrophoresis through the pores of a dynamically changing pore population.

Keywords: Electroporation; Molecular transport; Subpopulation; Heterogeneity; Flow cytometry; (Yeast)

1. Introduction

Electroporation is widely used as a research tool in biology, and increasing numbers of potential applications in biotechnology and medicine have been identified [1–3]. It is generally accepted that electroporation occurs if the transmembrane voltage, $U(t)$, reaches a value of several hundred or more mV, and that some type of temporary aqueous pathways ('pores') appear in the membrane due to the combined energy of thermal fluctuations ('kT energy') and membrane electric field energy ('electric energy') [4–7]. While the resulting electrical behavior (e.g., 'reversible electrical breakdown') and mechanical changes (e.g., 'rupture') have received considerable attention, it is net molecular transport that is most important to biological systems. Indeed, although the first report of greatly enhanced molecular transport appeared more than twenty years ago [8] understanding of electroporative molecular transport remains rudimentary.

Briefly, a number of previous studies have provided important information about molecular transport. Typically the experimental methods have involved measurements of (1) total populations of cells, e.g., involving radioactive substances, so that a population average result is obtained [9–11], or (2) single cells, e.g., imaging methods, which provide spatial and temporal resolution but can only examine one or a small number of cells, which may or may not be representative [12–17]. A complimentary method, flow cytometry, has been used in the present study, as it can make quantitative fluorescence determinations on large numbers of individual cells.

The great majority of molecules involved in biochemistry are polar, highly soluble in water, and cannot cross the cell membrane at a significant rate by dissolution and diffusion. This is fundamental, because of the large elec-

* Corresponding author. Fax: +1 (617) 2532514.

SSDI 0005-2736(94)00258-4

trostatic energy barrier associated with moving charge from an aqueous to a lipid environment [18]. A transmembrane aqueous pathway, or an active transport mechanism such as endocytosis [19], is therefore needed. The short time scale ($\tau_p \approx 300$ μs) of the pulses used here and in most electroporation protocols suggests that there is insufficient time for a significant active transport contribution. For this reason we assume that aqueous pathway ('pore') formation occurs, and that transport through the pores, provides the dominant contribution.

The hypothesis that transient aqueous pores are involved is consistent with a physical model that is based on two energy contributions to pore formation: (1) a stochastic contribution associated with thermal fluctuations, and (2) a deterministic contribution associated with the increase in electrostatic energy within the membrane as the transmembrane voltage, $U(t)$, increases. This model was originally introduced to explain artificial planar bilayer membrane behavior [4], and has begun to be extended to the problem of molecular transport [20,21]. The stochastic contribution to pore formation leads to the idea that electroporation fundamentally involves a pore population. Moreover, the evolution of such pores is believed to depend on the time course of transmembrane voltage, $U(t)$. A heterogeneous electroporation response is therefore expected within a cell suspension, mainly on physical grounds. In addition to the stochastic nature of pore formation, $U(t)$ is expected to vary over the cell membrane, and to depend on the size, shape and orientation of the cell [20]. For these reasons, molecular transport is expected to vary within a cell population (Table 1).

Here we used a small polar molecule (calcein) which is an established polar tracer [22], that ordinarily does not penetrate the cell membrane. The yeast *S. cerevisiae* was chosen because it is an asymmetric, budding microorganism that is significantly different from the almost-spherical red blood cell ghosts, that were used in similar studies of molecular transport [23,24]. Flow cytometry was employed in order to measure both forward light scatter (FS) and green fluorescence (GF), and is a well established bioanalytical method which routinely allows these measurements to be carried out at the rate of about 1000 cells per second [25,26]. By employing fluorescence calibration techniques which are appropriate for molecules which bind or reside essentially in solution with a cell [27], the net number of calcein molecules, N_s, transported into individual cells ('uptake'), within an electrically pulsed cell population was obtained.

2. Methods

The methods used here are extensions of those used previously [23,27–30]. The intent is to (1) obtain quantitative determinations of the uptake per cell, and (2) partially assess long term membrane recovery of individual cells.

Table 1
Expected sources of heterogeneous electroporation [3,20]

Source	Significance
Cell size	$\Delta U(t)$ depends on size
Cell shape	$\Delta U(t)$ depends on shape
Cell orientation	$\vec{E}_e$ a directional quantity
Membrane composition	Composition variation within cell population
Pore statistical behavior	Electroporation is fundamentally stochastic
Cell-cell separation	Perturbation of local field by nearby cells
Tissue heterogeneity	Perturbation of local field by tissue

Predicted sources of heterogeneous electroporation behavior. The basic expectation is that the time dependent transmembrane voltage, $U(t)$, is critical to the creation and evolution of a pore population. All but the last entry are relevant to cell suspensions, and the next to the last entry is expected to be unimportant if the average spacing between cells is large compared to a characteristic linear dimension of the cell. In the case of membrane composition, the experimentally observed onset of electroporation at about $U \approx 0.5$ to 1 V for many different types of membranes suggests that membrane composition is not particularly important for the initial phase of pore creation and evolution. Nevertheless, minor contributions to heterogeneity may be due to population variations of membrane properties. Furthermore, in contrast to onset, membrane recovery following membrane discharge (time scale $\approx 10^{-6}$ s) may be significantly affected by membrane composition. Thus, if metastable pores or other persistent transport mechanisms occur in some cells, this may also contribute to heterogeneity in molecular transport.

2.1. Overall pulsing, washing and measurement sequence

Immediately before pulsing, yeast were suspended in phosphate buffer (100 mM, pH 6.8) containing 1 mM calcein, and then placed in a pulsing cuvette. A single exponential pulse was then applied to the electrodes. Five minutes after the pulse, the sample was centrifuged (1000 $\times g$; 3 min) and washed twice with buffer containing 10 μM propidium iodide (PI). The exposure of the cells to this PI solution was maintained thereafter, including the time of flow cytometric analysis.

2.2. Cell preparation

Yeast (*S. cerevisiae*; ATCC, Rockville, MD, #2341) were cultured in YPD medium (10 g yeast extract, 20 g peptone, and 20 g dextrose in 1 L deionized water) at 27°C overnight. The cells were grown into the exponential phase before resuspension for pulsing. At the time of pulsing, the cell suspension concentration was $\rho \approx 1 \cdot 10^7$ cells ml^{-1}, so that using the relation $\rho = 1$ cell/s^3, the mean cell-cell spacing was $\bar{s} \approx 5 \cdot 10^{-3}$ cm ≈ 50 μm. Yeast cells are about 7 μm in length, so that the average cell separation was about seven cell lengths. At this separation cells should not significantly alter the electric field experienced by neighboring cells. In this sense, the suspension was dilute.

2.3. Fluorescent molecules

In order to make measurements at the individual cell level, two fluorescent molecules were used with flow cytometry.

Calcein (623 Da, $z = -4$ at pH 7, GF = green fluorescence; Molecular Probes, Eugene, OR, #C-481) was obtained as a powder. Fresh solutions of 1 mM calcein in phosphate buffer were made just before each experiment. Calcein is an established polar tracer which does not permeate cell membranes. Unlike fluorescein, the fluorescence of calcein is independent of pH over the range $6.5 < \text{pH} < 9.5$ [22]. This means that even though there is a small difference between the extracellular medium pH (buffer at pH 6.8) and the usual intracellular pH of *S. cerevisiae* of pH 6.7 [31], no correction for fluorescence is needed. As described below, a quantitative calibration relating GF magnitude to the equivalent number of calcein molecules was used.

Propidium iodide (PI; 668 Da, $z = +2$ at pH 6.8, RF = red fluorescence; Molecular Probes, #P-1304) was used to test for membrane integrity long after the pulse-induced transmembrane voltage increase decayed, in order to determine whether metastable pores or permanent holes existed. An important property of PI was exploited: upon binding to doubly stranded nucleic acids the RF intensity increases significantly. This property, and its exclusion by membranes because of its charge, are the basis for the widespread use of PI as a cell membrane integrity probe [25]. Somewhat arbitrarily PI was provided 5 min after pulsing, and then retained thereafter, including the time of flow cytometry. A quantitative calibration of RF magnitude was not made, as PI was not used to determine molecular transport. Instead PI was used to partially assess membrane recovery for the time interval starting 5 min after the pulse and ending at the time of flow cytometry.

2.4. Flow cytometry and fluorescence microscopy

Suspended yeast cells were analyzed with a Becton Dickenson FACStar^{Plus} using an argon laser 488 nm line at 100 mW excitation. Three optical parameters were measured: (1) FS = forward light scatter, which served as a trigger event and also provided an indicator of cell size and shape; (2) GF = green fluorescence, which was subsequently calibrated as an equivalent number of calcein molecules; and (3) RF = red fluorescence, which was used as an uncalibrated measurement of the PI which had entered cells. For each case FS, GF and RF were measured individually for $1 \cdot 10^4$ cells, and included a computed compensation for fluorescence spectral overlap.

In order to help interpret the flow cytometry results, combined fluorescence and ordinary light microscopy were used as needed to examine samples of pulsed and control yeast. In some cases samples of the entire pulsed cell population were examined. In other cases, yeast associated with particular subpopulations (e.g., based on FS and GF) were sorted onto microscope slides by using the cell sorting capability of the FACStar^{Plus}, and then visually inspected by fluorescence microscopy. Because yeast with significant GF were seen to be fluorescent throughout, and not just along the perimeter, we interpreted the GF as due to electroporative uptake of calcein rather than surface binding.

2.5. Data analysis and display

The raw data files for each flow cytometric analysis were transferred over a local network to a computer workstation (Sparcstation 2, Sun Microsystems, Mountain View, CA) for off-line analysis. For those cases where cell sorting was used, the sorted cells were promptly examined by fluorescence microscopy at the flow cytometry facility. Commercially available software associated with the FACStar^{Plus} was used to collect data and to perform flow sorting. Custom software was used to analyze the data, so that both contour plot representations of two-dimensional histograms (e.g., Fig. 4) and one-dimensional histograms (e.g., Fig. 3) could be calibrated to display uptake in number of calcein molecules, N_s.

2.6. Calibration of green fluorescence as an equivalent number of calcein molecules

Following a previous protocol [27] GF measurements were converted into an equivalent number of calcein molecules. Specifically, the number of calcein molecules, N_s, was determined by using FITC calibration beads (Flow Cytometry Standards, Research Triangle Park, NC) labeled with a known number of equivalent soluble fluorescein molecules. For each set of beads, the mean channel number was measured, and the number of equivalent soluble calcein molecules (ESCM) was calculated using the previously determined ratio (calcein fluorescence)/(free fluorescein fluorescence) $= 0.65 \pm 0.28$ [23]. This yielded a set of four number pairs (mean channel, log[ESCM]), to which a calibration line was fit. Whenever calibrated mean values are shown here, the mean value of the control has been subtracted, so that the mean of the control is zero. However, this is not the case for the contour plots and histograms. There are two reasons for this: (1) when the mean of the control is subtracted from the data points from the control sample, the data below the mean is negative, and thus can not be plotted on a log scale, and (2) the error introduced by not correcting for the background fluorescence is less than 10% in all cases except the control.

The RF measurements were used without such a calibration to determine the relative amount of PI entry into cells for $t \geq 5$ min after pulsing. Quantitative calibration was not used, because PI fluorescence was used for membrane recovery assessment rather than for electroporative uptake determinations.

2.7. Electric field pulse characterization

Here a single exponential electric field pulse was used, and only the amplitude of the pulse was altered. A Bio-Rad Gene Pulser (Richmond, CA) with standard Bio-Rad cuvettes (0.4 mm and 0.2 mm electrode spacing), which have aluminum electrodes, was used to deliver the pulses. Because of the possibility that significant potential drops can occur near the electrode/electrolyte interface, we did not use the nominal electric field (electrode voltage divided by the parallel plane electrode separation). Instead we computed the actual electric field within the electrolyte away from the electrodes, E_e, by measuring the current pulse through the cuvette, and then using the medium conductivity, σ_e (determined separately), to calculate E_e (unpublished results). The ratio of actual to nominal field, $E_{e,0}/E_{nominal}$, is between 0.5 and 0.8, depending on the applied voltage. The determination of the actual electric field experienced by the cells was made because of the generally strong and non-linear dependence of electroporation on field strength [30].

2.8. Determination of possible calcein loss during cell handling

The process of resuspending the cells prior to flow cytometry could possibly lead to loss of calcein previously taken up because of the electrical pulse. However, two membrane states should be considered: (1) recovered membranes that block calcein transport, and (2) nonrecovered or incompletely recovered membranes that pass calcein. The experimental protocol should not involve perturbations that cause release of calcein for recovered membranes, but loss of calcein should in fact occur if calcein can pass through the non-recovered or incompletely recovered membrane. The presence of PI for all $t \geq 5$ min after pulsing provided a test for cells which were significantly permeable. Cells with significant GF but insignificant RF were therefore interpreted as cells which had intact membranes for $t \geq 5$ min.

2.9. Temperature of cell suspension

The cell suspension temperature before pulsing was $T = 25 \pm 5$°C (nominal room temperature). Heating due to both ohmic dissipation within the bulk medium and at the electrode interface is expected.

2.10. Determination of the intra-/extracellular partition coefficient for calcein in S. cerevisiae

For interpretation of the quantitative uptake measurements, it was important to determine the relative solubility of calcein in the intra- and extracellular environments of the yeast cells. As described in detail below, we suspended yeast in a known calcein-containing phosphate solution, added methanol to permanently permeabilize the cells, waited for calcein to equilibrate between the intra- and extracellular regions, and then removed the cells from the (calcein-depleted) solution. By measuring the average cell volume, $\bar{V}_{cell}$, the number of cells, N_{cells}, the fluorescence, F_0, of the initial, pre-methanol permeabilization solution, and the fluorescence, F_f, of the depleted (final) calcein solution, we calculated the effective partition coefficient by using the following equation (derivation below)

$$g_{eff} = \frac{(F_0 - F_f)}{N_{cells}\bar{V}_{cell}F_f} + 1 \quad (1)$$

2.11. Determination of F_0 and F_f

Yeast were cultured as described previously and concentrated to yield a 37% (v/v) suspension. The cells were resuspended in a 1 mM solution of calcein in phosphate buffer (pH 6.8, 0.2 μ filtered, Gelman Sciences, Ann Arbor, MI, #4192). Two 0.5 ml aliquots were taken from this suspension.

The first aliquot was diluted 1:2 with buffer and centrifuged. The supernatant was then removed and diluted $1{:}10^4$ with buffer, so that the GF of calcein could be measured with a spectrofluorimeter (Fluorolog II, Spex Industries, Edison, NJ). The fluorescence emission was measured from 470 nm to 530 nm, which includes the 488 nm laser line used to excite the samples. We assumed that the contribution from the laser to the measured fluorescence is constant, so that the peak at 488 nm could be use to normalize each curve. After this normalization, the area under the curve was computed. Five independent dilutions and measurements were carried out, and the results were averaged in order to obtain F_0, of the supernatant before the cell membrane was permeabilized.

The second aliquot was diluted 1:2 with methanol in order to permeabilize the cells. After allowing the cells to remain in the methanol for 10 min, the suspension was gently centrifuged ($500 \times g$) for 20 min. The supernatant was removed, and centrifuged ($13\,000 \times g$) to remove any cellular debris. The resulting supernatant was then also diluted by a factor of 10^4, and the GF of calcein measured in the spectrofluorimeter. Again five independent dilutions were made and the results averaged. This procedure yielded the fluorescence, F_f, of the supernatant after the cell membrane was permeabilized.

2.12. Determination of $\bar{V}_{cell}$

A resistive particle sizing method (Coulter Counter Model Z_F with Channelizer, Coulter Electronics, Hialeah, FL) was used to determine the average, effective radius of the yeast cells, as if they were spherical. This method has been found by others to provide a reasonable volume determination even for the non-spherical *S. cerevisiae*

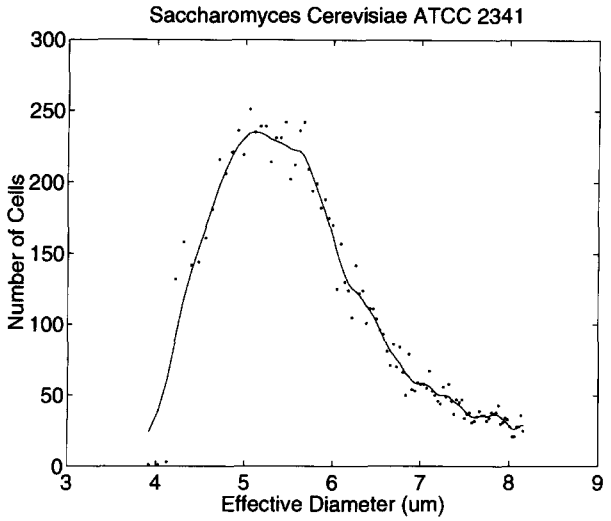

Fig. 1. Histogram of effective diameter of yeast cells as determined by a Coulter Counter, which has been found by others to provide a reasonable volume determination even for the non-spherical *S. cerevisiae* [32,34], because the Coulter method is primarily a volume-sensitive method [35]. These measurements were obtained in order to calculate the average yeast cell volume. Using the mean diameter, $2\bar{r}_{cell} = 5.8$ μm, the computed volume is $\bar{V}_{cell} = 1.0 \cdot 10^2$ μm^3 (10^{-10} cm^3).

[32–34]. This is a reasonable approach because this method is fundamentally responsive to the volume of the cell [35]. These measurements (Fig. 1) were obtained in order to calculate the average yeast cell volume, $\bar{V}_{cell}$. Using the mean effective diameter, $2\bar{r}_{cell} = 5.8$ μm, the computed volume is $\bar{V}_{cell} = 4\pi\bar{r}^3/3 = 1 \cdot 10^2$ μm^3 ($1 \cdot 10^{-10}$ cm^3). This agrees with a simple geometric estimate (below) which treats the yeast as an ellipsoid.

Microscopy confirmed that the yeast organisms were single or budding volumes that can be reasonably approximated as ellipsoids. The volume of an ellipsoid with circular cross-section is $V_{ellipsoid} = 4/\pi\ a^2 b$, where a and b are the minor and major ellipse axes. For single yeast (no bud) $a \approx 3$ μm and $b \approx 7$ μm. The corresponding volume is $V_{yeast,min} \approx (4)(3 \cdot 10^{-4}\ cm)^2(7 \cdot 10^{-4}\ cm)/\pi \approx 0.8 \cdot 10^{-10}$ cm^3. This calculated value is only a guide; the close numerical agreement with the Coulter counter value, which was actually used in our estimate, is believed fortuitous.

2.13. Determination of N_{cells}

The concentration of cells was measured by using a haemocytometer (counting about 200 cells; 9 aliquots) and then averaging. Using this value as a calibration, a Coulter Counter was adjusted to give approximately the same counts per volume, and then used to rapidly count cells from other samples. The Coulter Counter operating parameters were (1) aperture size = 50 μm, (2) 1/amplification = 8, (3) 1/aperture current = 1 (0.5 mA), and (4) threshold setting = 5.

2.14. Numerical value of g_{eff}

The experimentally determined values were substituted into the preceding equation to give

$$g_{eff} = \left[\frac{(F_0 - F_f)}{N_{cells}\bar{V}_{cell}F_f} + 1\right] = 2.8 \pm 1.5 \qquad (2)$$

This value is slightly greater than one, and is therefore interpreted as the negatively charged calcein having a slight preference to reside within the intracellular compartment The fact that g_{eff} is close to one is consistent with the accepted use of calcein as a polar tracer, which would not be the case if there were significant binding of calcein to intracellular constituents. If g_{eff} were less than one, a 'repulsion' of calcein from the cell interior would have been involved, and this could have contributed to the result $\bar{N} < N\bar{V}[calcein]_{supply}$. However, given the finding that $g_{eff} > 1$, this cannot be the explanation.

2.15. Derivation of the partition coefficient expression

Here we derive the expression used to calculate g_{eff}, the effective partition coefficient for intra- and extracellular calcein under our conditions. This expression involves only four measured quantities: two solution fluorescence measurements (1) F_0 = fluorescence emission of the 1 mM calcein solution (the pulsing medium), and (2) F_f = fluorescence emission of the supernatant after chemical permeabilization and removal of cells, along with (3) the volume of the cells, and (4) the number of cells in the solution.

$$g_{eff} \equiv \frac{[calcein]_{in,f}}{[calcein]_{out,f}} \text{ with the constraint}$$

$$N_{in} + N_{out} = N_{tot} \text{ for calcein molecules} \qquad (3)$$

The subscripts 'out' and 'in' denote 'extracellular' and 'intracellular' respectively.

The intracellular concentration cannot be reliably measured directly, because of unknown contributions of light scattering and light absorption due to cellular material. For this reason the following relation was used, which indirectly determined $[calcein]_{in,f}$ by expressing and g_{eff} as

$$g_{eff} = \frac{(N_{tot} - N_{out,f})}{V_{cells}} \frac{V_{out,f}}{N_{out,f}} \qquad (4)$$

where $N_{tot} = V_{tot}[calcein]_{out,i}$ is the total number of calcein molecules present. Similarly, after chemical permeabilization $N_{out,f} = V_{tot}[calcein]_{out,f}$. We can use the expressions

$$N_{tot} = \frac{V_{tot}F_0}{K_F} \text{ and } N_{out,f} = \frac{V_{out,f}F_f}{K_F} \qquad (5)$$

where K_F is the calibration coefficient relating fluorescence emission to calcein concentration, and the relationship $V_{out} = V_{total} - N_{cells}\bar{V}_{cell}$ to enable us to express the

partition coefficient in terms of measured quantities. Note that because ratios are involved, the fluorescence calibration coefficient does not explicitly appear.

$$g_{\text{eff}} = \frac{(V_{\text{tot}}F_0 - V_{\text{out,f}}F_{\text{f}})}{V_{\text{cells}}F_{\text{f}}} = \frac{\left(V_{\text{tot}}F_0 - \left[V_{\text{tot}} - N_{\text{cells}}\bar{V}_{\text{cell}}\right]F_{\text{f}}\right)}{N_{\text{cells}}\bar{V}_{\text{cell}}F_{\text{f}}} = \frac{F_0 - F_{\text{f}}}{N_{\text{cells}}\bar{V}_{\text{cell}}F_{\text{f}}} + 1 \quad (6)$$

The partition coefficient is expected to depend on the fluorescent molecule (here calcein), the cell type (here *S. cerevisiae*), the pulsing and/or recovery medium (here phosphate buffer), and the temperature (here 25°C).

2.16. Calculation of the number of molecules at equilibrium

In the actual electroporative uptake experiments the supplied extracellular calcein concentration was 1 mM = $6 \cdot 10^{17}$ molecules ml^{-1}. At a typical cell concentration of $\rho = 3 \cdot 10^7$ cells ml^{-1} the total cell volume per ml of pulsed cell suspension was $V_{\text{cells,pulsed}} = (3 \cdot 10^7 \text{ cells})(1 \cdot 10^{-10} \text{ ml cell}^{-1}) = 3 \cdot 10^{-3}$ ml. This is only 0.3% of the volume. Thus, even if the cells were to equilibrate with the extracellularly supplied solution, the external solution would be depleted in calcein by less than 1%. With this in mind, the undepleted concentration was used, and the number of molecules at equilibrium within the average cell volume was calculated as

$$\bar{N}_{\text{s,equil}} \equiv \bar{V}_{\text{cell}}C_{\text{calcein}} \approx (1.0 \cdot 10^{-10} \text{ ml})(6 \cdot 10^{17} \text{ molecules ml}^{-1}) = 6 \cdot 10^7 \text{ molecules} \quad (7)$$

In contrast, a typical experimental value for the subpopulation with the largest uptake was $\bar{N}_{\text{s}} = 1.5 \cdot 10^6$ molecules. The ratio of the experimental value to this 'theoretical value' is

$$R \equiv \frac{\bar{N}_{\text{s}}}{\bar{N}_{\text{s,equil}}} \approx \frac{1.5 \cdot 10^6}{6 \cdot 10^7} = 2.5 \cdot 10^{-2} \quad (8)$$

which at 2.5% is far from the equilibrium value. This is important to interpreting the quantitative uptake results.

3. Results and discussion

We have obtained quantitative determinations of molecular uptake at the individual cell level for an elongated, budding microorganism, and have partially assessed membrane recovery of the same cells. The individual cell data are presented as one- and two-dimensional histograms, which reveal significant subpopulations with respect to both uptake and membrane recovery. Moreover, the subpopulations which are present vary significantly as the electric field pulse magnitude is changed.

3.1. Quantitative molecular uptake and membrane recovery per cell

All of the uptake data are reported in terms of N_{s}, the number of calcein molecules taken up by an individual cell of the yeast *Saccharomyces cerevisiae*. Although *S. cerevisiae* is a budding microorganism, which often consists of a mechanically connected parent cell and bud, but with separate cytosolic compartments, we nevertheless considered this parent-bud entity as a single cell. This is the entity that triggered a GF measurement. Traditionally, it is also the entity counted by conventional methods such as viable plating, as most of the colony forming units are single parent-bud entities. As shown in Figs. 3 and 4, N_{s} was found to have a significant variation (population distribution) within the statistically significant population samples of 10^4 cells. For electric fields large enough to cause measurable uptake, the uptake distribution usually varied by a factor of 10 (from 10% to 90%).

In addition to the striking subpopulation changes, another significant finding is the behavior of $\bar{N}_{\text{s}}$ as a function of pulse magnitude, $E_{\text{e,0}}$. Even though the yeast cells are non-spherical, and two distinct net uptake subpopulations were observed, both subpopulations had a maximum uptake per cell that was far below the simple equilibrium value. This is consistent with the following hypothesis: (1) for most cells that experience electroporation, N_{s} reaches a maximum value for the single pulse because of fundamental behavior of molecular transport through a transient pore population [20,21], and (2) two subpopulations with respect to membrane recovery and a corresponding loss of calcein ensue, such that one subpopulation (large uptake) retains essentially all of the calcein originally taken up, and the other subpopulation (small uptake) has about 10% of the originally acquired calcein. Our interpretation is that for these cells the membrane does not recover sufficiently to prevent calcein from escaping, and the remaining approx. 10% is loosely bound within the cell.

This interpretation is plausible, in light of the following additional information. First, red blood cell ghosts, which are essentially biological membranes enclosing an aqueous electrolyte, also exhibit a non-equilibrium uptake plateau for a similar, single pulse protocol [23,24]. This suggests that a membrane response alone is involved, and not an active transport process stimulated by the electric field pulse as has been observed in some cases [19]. Moreover, an electroporation theory based solely on transient aqueous pores in a small, constant area, planar bilayer membrane predicts that for small charged molecules the transport will first rise with $E_{\text{e,0}}$, and then actually decrease slightly, thus approximating a plateau [21]. This appears to be due to an

almost constant transmembrane voltage during most of a large exponential pulse [21,36]. Second, the use of PI to test for membrane integrity by supplying PI five minutes after the pulse, and retaining PI thereafter, showed that PI uptake occurred in the small uptake subpopulation, but not in the large uptake subpopulation. This is direct support for the hypothesis. Taken together, therefore, the hypothesis is plausible.

Examination of the FS data (Fig. 2) shows that no significant change in FS occurred, whereas GF histograms (Fig. 3) did change as a result of electric field pulses. This is consistent with the interpretation that molecular uptake occurred via small membrane changes that did not significantly alter the size and shape of the cells. A total of 10^4 yeast cells were measured for each experimental condition.

3.2. Interpretation of calcein uptake subpopulations

The emergence of two calcein peaks in Fig. 3 is interpreted as follows: the minor peak is due to release of previously acquired calcein because of a leaky membrane, while the major peak has cells with recovered (for calcein transport) membranes. This is further supported by the data presented in Fig. 4 (see also Fig. 5), as the subpopulations E, F, and G all have cells admitting significant PI, while subpopulations A, B and C all have insignificant PI entry. In considering the PI uptake results, note that the samples were pulsed sequentially, with the addition of PI 5 min after the pulse. Because there were 12 samples, pulsing and washing took 70 min, and so there is a difference of 70 min in the time from PI addition to flow cytometry analysis for the first and last samples. Flow cytometry was done 10 min after the experiment was completed, so that the range of PI exposure times was 20 to 90 min.

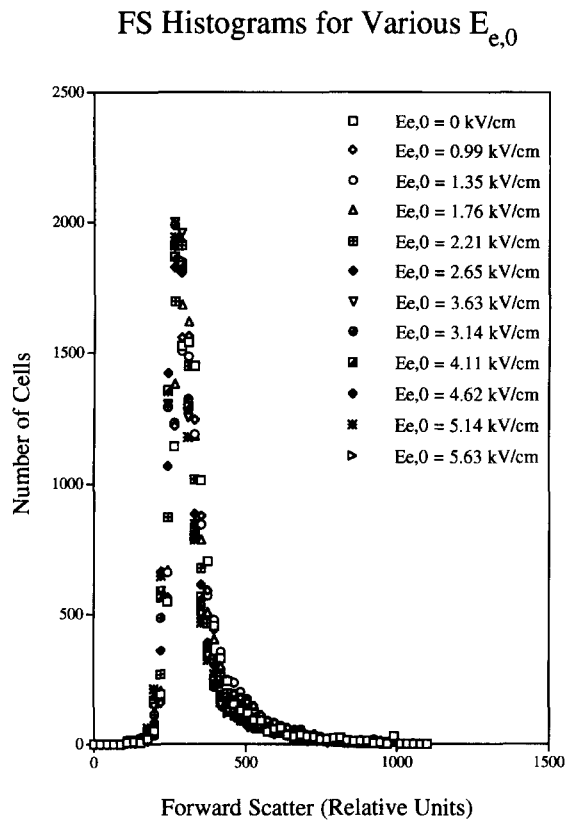

Fig. 2. Cell morphology distributions in the form of $\log_{10}$ (FS) histograms (one-dimensional population distributions). Each of these histograms is based on analysis of $1 \cdot 10^4$ cells after a single pulse of the indicated electric field magnitude, $E_{e,0}$. The field values have been corrected for localized electrode/electrolyte potential drops (unpublished results). The forward scatter (FS) signal at 488 nm was used as a morphology/size indicator. More specifically, the FS was used as (1) a trigger, so that small scatter events (e.g., debris) would not be analyzed, and (2) a confirmation that yeast-size entities were analyzed. These data show that the morphology of the yeast did not change significantly due to application of the electric field.

For the case $E_{e,0} = 1.0$ kV/cm and larger, the log histogram exhibited a peak which occurred at larger N_s values as $E_{e,0}$ increased. This is plausible behavior, as with increasing field strength both more and larger pores, and greater electrical drift transport, might be expected. But for the case $E_{e,0} = 2.7$ kV/cm and larger, an unexpected second peak appeared, which had about ten-fold less uptake. The sorting capability of the flow cytometer was used to isolate the cells of both the large uptake and small uptake peaks. Fluorescence microscopy of cells sorted from these subpopulations showed that in both cases the cells had uniformly green fluorescence, but with the small uptake peak simply having much dimmer cells. This observation ruled out the possibility that somehow only one of the parent-bud entity was contributing (e.g., a hypothetical possibility was that the larger parent had experience rupture of a portion of its membrane, resulting in calcein loss from the larger parent). The fact that both parent and bud have uniform but weaker fluorescence is surprising, and previously unexplained.

At progressively larger $E_{e,0}$, the large uptake peak has essentially the same GF, but diminishes in size. This means that the subpopulation with large uptake has about the same uptake per cell, but the number of cells in this subpopulation diminishes. Simultaneously the small uptake peak remains in about the same location (peak values of $N_s(3.1 \text{ kV cm}^{-1}) = 3.4 \cdot 10^5$ molecules, $N_s(4.6 \text{ kV cm}^{-1}) = 3.4 \cdot 10^5$ molecules, and $N_s(5.6 \text{ kV cm}^{-1}) = 5.6 \cdot 10^5$ molecules).

The data of Fig. 4 support the interpretation of the small uptake peak as due to cells which have permanently leaky membranes. That data shows the RF due to propidium iodide (PI) that was supplied extracellularly at least 20 min prior to flow cytometric analysis. PI is a widely used membrane integrity probe, and ordinarily does not cross the cell membrane [25]. We interpret the entry of PI as due to permanent opening of the membrane at some time after the electroporating pulse. In this interpretation, cells which previously took up large numbers of calcein molecules subsequently lost most of them, as the membrane either did not recover or subsequently opened.

Figs. 6 and 7 show the mean calcein uptake, $\bar{N}_s$, for

different electric field values. The finding of a plateau in average net uptake for large field strengths is particularly significant. As shown in Fig. 6 there is a region where $\bar{N}_s$ increases with E_e, followed by a region where $\bar{N}_s$ is independent of field strength. Similar observations were made using red blood cell ghosts, in which flow cytometry was used to determine the uptake of calcein, lactalbumin and bovine serum albumin for a variety of exponential pulsing conditions [23,24]. For these ghost experiments the mean uptake was also significantly less than 'equilibrium

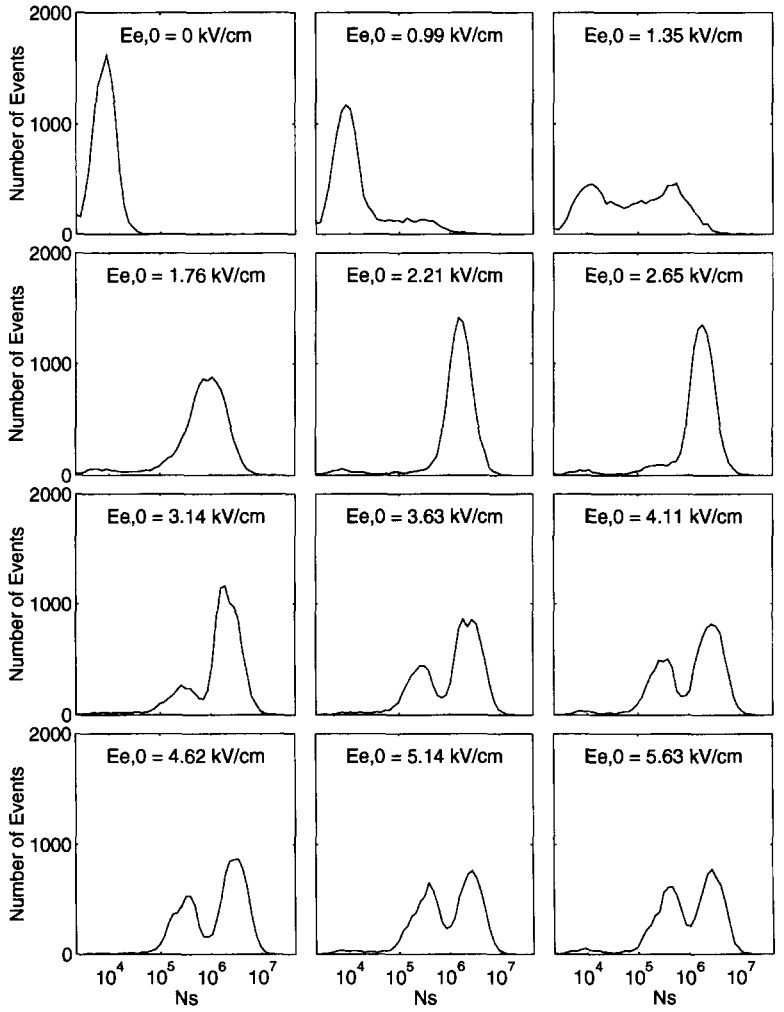

Fig. 3. Series of $\log_{10}$ (N_s) histograms where N_s is interpreted as the net number of calcein molecules taken up by individual cells based on a calibration that relates total cell green fluorescence to N_s. Inspection of the control ($E = 0$ kV/cm) shows that the average contributions of non-specific staining, cell autofluorescence and instrumental noise was equivalent to about 10^4 calcein molecules. The panels show the population distributions for increasing $E_{e,0}$ from zero (control) to 6 kV cm^{-1}. These data show that there are subpopulations with respect to uptake, and that major changes occur as $E_{e,0}$ is varied. Specifically, inspection of these data shows that for $E_{e,0} \geq 3$ kV/cm there are always two major subpopulations for which the FS signal range is about the same, but two distinct ranges of N_s are evident. Our interpretation of the progression of changes is as follows. $E_{e,0} = 0$: control, which gives the distribution of background fluorescence of yeast cells exposed to the calcein solution. Both cellular autofluorescence and non-specific staining by calcein are expected. $E_{e,0} = 1$ kV/cm: lower end of an approximate threshold for uptake for these particular conditions, as emergence of a small subpopulation with significant N_s over the background distribution is evident. Initial inspection of these results might suggest that the use of a log scale could cause an apparent variation in uptake. However, the variations are real and large; for example, here ranging from $N_s \approx 3 \cdot 10^4$ to almost $N_s = 10^6$ molecules per cell. $E_{e,0} = 1.4$ kV/cm: participation of most cells in uptake, as 75% of the cells have fluorescence equivalent to or greater than $N_s \approx 1.6 \cdot 10^4$ molecules/cell. The distribution is broad, with an almost triangular peak when displayed on this log scale. $E_{e,0} = 1.8$ kV/cm: upper end of an approximate threshold for uptake for these particular conditions, as almost all cells now participate in calcein uptake. A single, broad distribution occurs, with $\bar{N}_s \approx 10^6$ molecules/cell, but ranges from about 10^5 to about $7 \cdot 10^6$. A small, non-participating subpopulation with the control range of N_s values is also present. $E_{e,0} = 2.2$ kV/cm: a sharper distribution in uptake exists, $\bar{N}_s \approx 2 \cdot 10^6$ molecules/cell, but ranges from about $6 \cdot 10^5$ to about $5 \cdot 10^6$, and a very small non-participating subpopulation is present. $E_{e,0} = 2.7$ kV/cm: a slightly broader distribution, with a small, almost flat shoulder on the left. Here $\bar{N}_s \approx 2.2 \cdot 10^6$ molecules/cell, but (including the shoulder) ranges from about 10^5 to about 10^7. Again a very small non-participating subpopulation is present. $E_{e,0} = 3.1$ kV/cm: two distinct peaks, with $\bar{N}_s \approx 3 \cdot 10^6$ molecules/cell, for the large uptake subpopulation, and $\bar{N}_s \approx 3 \cdot 10^5$ molecules/cell, for the small uptake subpopulation, but no significant non-participating subpopulation is evident. $E_{e,0} = 3.6$ kV/cm through 5.6 kV/cm: a progressive shift as the pulse magnitude is increased further, with the small uptake subpopulation growing at the expense of the large uptake subpopulation until the last two panels, for which the small and large uptake subpopulations are comparable. Often no significant non-participating subpopulation is evident.

uptake', i.e., much less than the ghost volume multiplied by the extracellular concentration. Given that only two types of cell membrane have exhibited a plateau, it is not yet established that this behavior is general. Interestingly, however, a theoretical model based solely on transient aqueous pores is consistent with both known electrical behavior (e.g., reversible electrical breakdown) and an approximate plateau in molecular transport [21]. The theoretical model also predicts a counter-intuitive behavior of the transmembrane voltage, $U(t)$. For an exponential pulse that causes 'reversible electrical breakdown', U drops suddenly when the membrane achieves a large conductance, but then temporarily almost ceases falling for a time $t \approx \tau_p$, even though the exponential pulse itself decays without interruption to zero [21,36]. According to the theoretical model prediction the magnitude of U at this 'pause' is independent of the magnitude of the exponential pulse [36], and this is qualitatively consistent with pulse magnitude-independent molecular transport which is driven through pores by the local electric field across the membrane.

A significant expected finding is confirmation of quite heterogeneous uptake. The large shifts in the population distributions of uptake with increasing electric field strength was not anticipated in any detail, but the existence of changes is not surprising. In spite of the marked hetero-

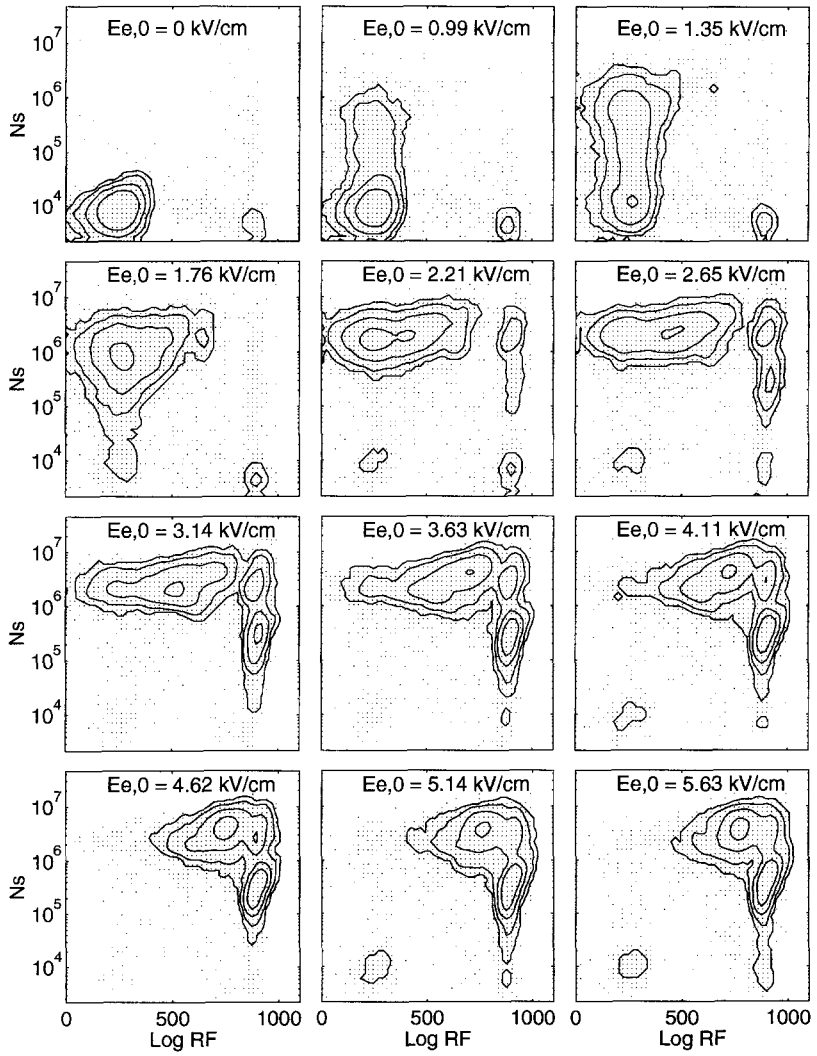

Fig. 4. Calcein uptake and red fluorescence (RF) associated with propidium iodide (PI) uptake due to its delayed addition (prior to flow cytometry) in the form of $\log_{10}(N_s) - \log_{10}(\mathrm{RF})$ contour plots. Each contour line an iso-frequency-of-occurrence line; four contours are used in each panel, with the values of 2.1, 6.1, 10 and 20 events (cells). Again, each of these two-dimensional histograms is based on analysis of $1 \cdot 10^4$ cells after a single pulse. Here PI is used in its usual role of membrane integrity probe, so that cells with large RF are interpreted as having non-recovered membranes. As described further in Fig. 5, as $E_{e,0}$ is increased, there are two major subpopulations (A and B) one minor subpopulation (C), and sometimes a diffuse additional subpopulation (D). Visual inspection of the data at any one field strength allows boundaries to be drawn which distinguish these subpopulations, so that computer analysis of these subpopulations can determine the percentage of cells in each subpopulation (Fig. 5). Although useful qualitatively, the fact that the subpopulation boundaries change with $E_{e,0}$ has the consequence that quantitative trends cannot be justifiably extracted. Nevertheless, manually selected boundaries were used to obtain some idea of the size of these subpopulations, and these are presented in Fig. 5.

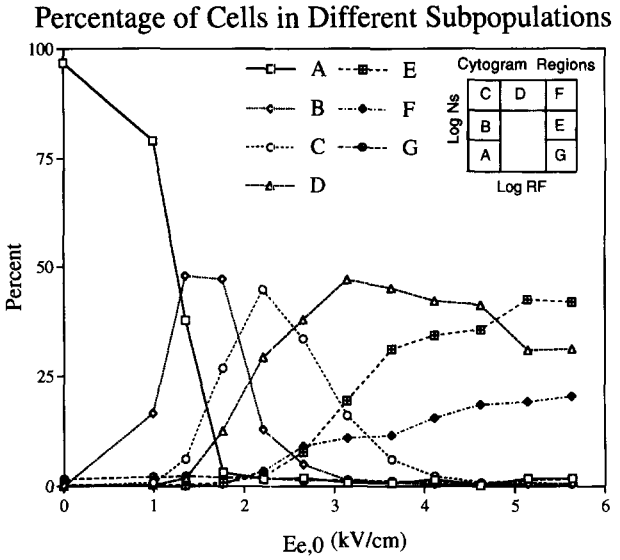

Fig. 5. Graphical presentation of the shift in subpopulations with electric field pulse magnitude, $E_{e,0}$, which was obtained by using a series of defined regions ('Cytogram Regions') in the $\log_{10}(N_s) - \log_{10}$ (RF) space. The 'unaffected' subpopulation [A] drops rapidly, and has essentially vanished by $E_{e,0} = 2$ kV/cm. The other $\log_{10}(N_s) - \log_{10}$ (RF) regions begin to be occupied within the range 1 to 2 kV/cm, so that for this particular pulse this range is an approximate threshold. As clearly shown in Figs. 3 and 4, and presented here with quantitative indices (percentages) the total cell population exhibits extremely heterogeneous behavior, with a complex series of subpopulations emerging and then retreating as only the pulse magnitude is varied.

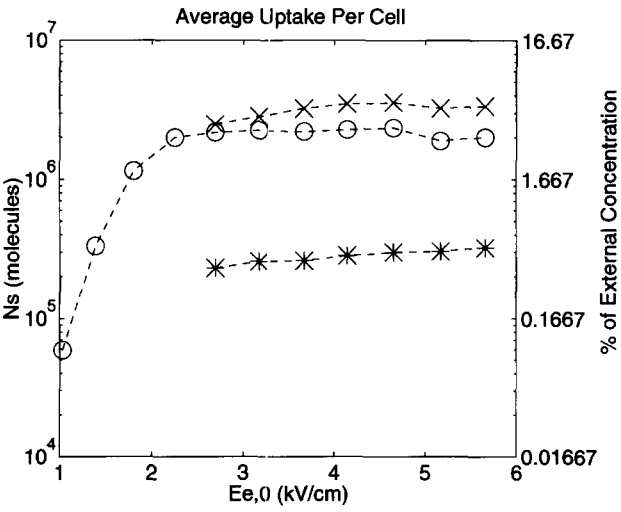

Fig. 6. The arithmetic average (mean) uptake per cell for three populations: ○= Total population (all cells analyzed), x = large uptake per cell (peak with high GF in Fig. 3), and * = small uptake per cell (peak with low GF in Fig. 3). The population average curve rises from background values within the 1 to 1.5 kV/cm region, achieves a maximum, and then falls slightly. This high field decrease is due to increasing numbers of cells in the 'smaller uptake' subpopulation (Figs. 3 and 4). The 'high GF' and 'low GF' curves have the interesting feature that an approximate plateau is reached for both the 'high GF' and 'low GF' subpopulations. The corresponding mean numbers of calcein molecules are $\bar{N}_s \approx 3 \cdot 10^6$ molecules/cell for the 'high GF' subpopulation, and $\bar{N}_s \approx 3 \cdot 10^5$ molecules/cell for the 'low GF' subpopulation. Note that even the 'high GF' case has $\bar{N}_s \approx \ll N_{equilibrium} = 6 \cdot 10^7$ molecules/cell.

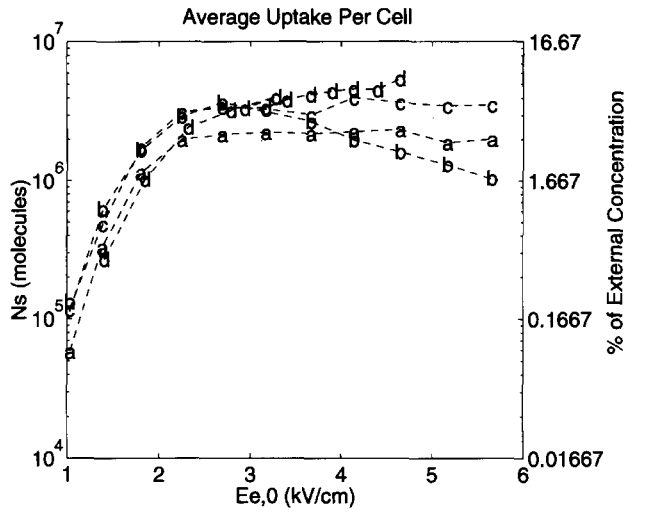

Fig. 7. Average number of calcein molecules taken up per cell (total population analyzed), $\bar{N}_s$, as a function of field strength for four different experiments. For $E_{e,0} < 1$ kV/cm the average uptake was essentially the zero, as the GF was not significantly different from the GF due to the combination of non-specific staining and cell autofluorescence. A quasi-plateau is found for $E_{e,0}$ greater than about 2.5 kV/cm, with uptake reaching a maximum at about 2.5 kV/cm, and then declining slightly.

geneity, the computed average uptake has two significant features: (1) a plateau is found, for the approximate range $3 \leq E_{e,0} \leq 6$ kV/cm, and (2) the significant changes in the large uptake and small uptake peaks is not at all revealed by the average. This surprising behavior is an explicit example of the danger in measuring only population averages in electroporation experiments. Likewise, it shows that there is no assurance that measurements on only one or a small number of individual cells will provide a complete understanding. Clearly there can be significant heterogeneity in electroporative behavior at any one electric field strength, and major shifts in subpopulations can occur as the field strength is varied.

More specifically, the population distributions of calcein uptake by individual cells show several subpopulations, which are characterized by differences in N_s (Figs. 3 and 4). This means that both the net uptake and the extent of membrane recovery vary from cell to cell. Moreover, the subpopulations change markedly as the pulse magnitude, $E_{e,0}$ is varied.

In summary, non-spherical cells that are widely spaced exhibit a large and complex degree of heterogeneity in their molecular uptake due to electroporation. Such behavior can only be understood fully if individual cell analysis is used with large numbers of cells, so that the various subpopulations can be resolved. In spite of the complexity of behavior it was also found that for the exponential pulses used here, molecular transport of calcein reaches a plateau that is far below the equilibrium value. This is interpreted as probably due to fundamental and counter-intuitive behavior of a highly interactive pore population, in which the transmembrane voltage throughout most of an

exponential pulse (one or two time constants) is almost constant.

Acknowledgements

We thank M.R. Prausnitz, U. Pliquett, G.I. Harrison, D. Cho, and V.G. Bose for stimulating discussions and technical assistance. This work supported by NIH Grant GM34077, Army Research Office Grant No. DAAL03-90-G-0218, and the DoD-University Research Instrumentation Program (Grant DAAG29-84-G-0066).

References

[1] Chang, D.C., Chassy, B.M., Saunders, J.A. and Sowers, A.E. (1992) Guide to Electroporation and Electrofusion, Academic Press, New York.
[2] Blank, M. (1993) Electricity and Magnetism in Biology and Medicine, San Francisco Press, San Francisco.
[3] Weaver, J.C. (1993) J. Cellular Biochem. 51, 426–435.
[4] Abidor, I.G., Arakelyan, V.B., Chernomordik, L.V., Chizmadzhev, Y.A., Pastushenko, V.F. and Tarasevich, M.R. (1979) Bioelectrochem. Bioenerg. 6, 37–52.
[5] Weaver, J.C. and Mintzer, R.A. (1981) Phys. Lett. 86A, 57–59.
[6] Glaser, R.W., Leikin, S.L., Chernomordik, L.V., Pastushenko, V.F. and Sokirko, A.I. (1988) Biochim. Biophys. Acta 940, 275–287.
[7] Barnett, A. and Weaver, J.C. (1991) Bioelectrochem. Bioenerg. 25, 163–182.
[8] Neumann, E. and Rosenheck, K. (1972) J. Membr. Biol. 10, 279–290.
[9] Kinosita, K. Jr. and Tsong, T.Y. (1977) Nature 268, 438–441.
[10] Kinosita, K. Jr. and Tsong, T.Y. (1978) Nature 272, 258–260.
[11] Teissie, J. and Tsong, T.Y. (1981) Biochemistry 20, 1548–1554.
[12] Mehrle, W., Zimmermann, U. and Hampp, R. (1985) FEBS Lett. 185, 89–94.
[13] Sowers, A.E. and Lieber, M.R. (1986) FEBS Lett. 205, 179–184.
[14] Liang, H., Purucker, W.J., Stenger, D.A., Kubiniec, R.T. and Huie, S.W. (1988) BioTechniques 6, 550–558.
[15] Dimitrov, D.S. and Sowers, A.E. (1990) Biochim. Biophys. Acta 1022, 381–392.
[16] Tekle, E., Astumian, R.D. and Chock, P.B. (1991) Proc. Natl. Acad. Sci. USA 88, 4230–4234.
[17] Sixou, S. and Teissie, J. (1993) Bioelectrochem. Bioenerg. 31, 237–257.
[18] Parsegian, V.A. (1969) Nature 221, 844–846.
[19] Zimmermann, U., Schnettler, R., Klöck, G. and Watzka, H. (1990) Naturwissenschaft 77, 543–545.
[20] Weaver, J.C. and Barnett, A. (1992) In Guide to Electroporation and Electrofusion (Chang, D.C., Chassy, B.M., Saunders, J.A. and Sowers, A.E., eds.), pp. 91–117, Academic Press, New York.
[21] Wang, M.A., Freeman, S.A., Bose, V.G., Dyer, S. and Weaver, J.C. (1993) In Electricity and Magnetism in Biology and Medicine (Blank, M., ed.), pp. 138–140, San Francisco Press, San Francisco.
[22] Haugland, R.P. (1992) Handbook of Fluorescent Probes and Research Chemicals, Molecular Probes, Eugene.
[23] Prausnitz, M.R., Lau, B.S., Milano, C.D., Conner, S., Langer, R. and Weaver, J.C. (1993) Biophys. J. 65, 414–422.
[24] Prausnitz, M.R., Milano, C.D., Gimm, J.A., Langer, R. and Weaver, J.C. (1994) Biophys. J. 66, 1522–1530.
[25] Shapiro, H.M. (1988) Practical Flow Cytometry, Second Edition, A.R. Liss, New York.
[26] Givan, A.L. (1992) Flow Cytometry: First Principles, Wiley-Liss, New York.
[27] Bartoletti, D.C., Harrison, G.I. and Weaver, J.C. (1989) FEBS Lett. 256, 4–10.
[28] Weaver, J.C., Bliss, J.G., Harrison, G.I., Mourant, J.R. and Powell, K.T. (1987) Electroporation in Individual Cells: Measurements Using Light Scattering and Fluorescence by Flow Cytometry. Proceedings 9th IEEE/Engineering in Medicine and Biology Society, pp. 708–709.
[29] Weaver, J.C., Harrison, G.I., Bliss, J.G., Mourant, J.R. and Powell, K.T. (1988) FEBS Lett. 229, 30–34.
[30] Bliss, J.G., Harrison, G.I., Mourant, J.R., Powell, K.T. and Weaver, J.C. (1988) Bioelectrochem. Bioenerg. 19, 57–71.
[31] Ryan, J.P. and Ryan, H. (1972) Biochem. J. 128, 139–146.
[32] Kubitschek, H.E. and Friske, J.A. (1986) J. Bacteriol. 168, 1466–1467.
[33] Johnston, G.C. (1977) J. Bacteriol. 132, 738–739.
[34] Van Huynh, N., Guns, M. and Decleire, M. (1989) Microbios 57, 41–48.
[35] Melamed, E.R., Lindmo, T., and Mendelsohn, M.L. (1990) Flow Cytometry and Sorting, Second Edition, Wiley-Liss, New York.
[36] Freeman, S.A., Wang, M.A. and Weaver, J.C. (1994) Biophys. J. 67, 42–56.